Journal of Physics and Chemistry of Solids 136 (2020) 109192

Contents lists available at ScienceDirect

Journal of Physics and Chemistry of Solids

journal homepage: http://www.elsevier.com/locate/jpcs

First-principle calculation for inherent stabilities of Li_xCoPO_4, Na_xCoPO_4 and the mixture $Li_xNa_yCoPO_4$

Abdelaziz M. Aboraia [a,b,*], V.V. Shapovalov [a], K. Vetlitsyna-Novikova [a], A.A. Guda [a], V. V. Butova [a,c], H.Y. Zahran [d,e], I.S. Yahia [d,e], A.V. Soldatov [a]

[a] The Smart Materials Research Institute, Southern Federal University, Sladkova 178/24, 344090, Rostov-on-Don, Russia
[b] Department of Physics, Faculty of Science, Al-Azhar University, Assiut, 71542, Egypt
[c] Federal Research Center of the Southern Scientific Center of the Russian Academy of Sciences, 344006, Rostov-on-Don, Russia
[d] Advanced Functional Materials & Optoelectronic Laboratory (AFMOL), Department of Physics, Faculty of Science, King Khalid University, P.O. Box 9004, Abha, Saudi Arabia
[e] Metallurgical Lab., Nanoscience Laboratory for Environmental and Bio-medical Applications (NLEBA), Semiconductor Lab., Physics Department, Faculty of Education, Ain Shams University, Roxy, 11757, Cairo, Egypt

ARTICLE INFO

Keywords:
Cathode material
Na-ion battery
Microwave-assisted synthesis
GGA+U
Olivines
Bader charge analysis

ABSTRACT

We have synthesized $NaCoPO_4$ and $LiCoPO_4$ via microwave-assisted solvothermal synthesis. The local atomic structure around Co atoms was characterized by means of Co K-edge XANES spectroscopy. Using X-ray diffraction, we have identified two $NaCoPO_4$ phases with Pnma and $P6_5$ space groups (lattice parameters a = 10.26 Å, b = 5.93 Å, c = 4.74 Å, and a = 10.16 Å,b = 10.16 Å,c = 23.87 Å, respectively) and one $LiCoPO_4$ phase has Pnma space group with lattice parameters a = 10.22 Å, b = 5.93 Å and c = 4.71 Å. Within GGA + U approximation we have calculated the variation of the cell voltage versus Li foil and atomic Bader charges for a wide range of alkali metal concentration in the material. Considering the low cost of the material and high intercalation voltage the synthesized sodium-based material is a good candidate for novel cathode materials.

1. Introduction

The problem of energy storage and recyclable use of small and powerful accumulators is the main challenge for the intense development of electric vehicles, mobile devices, autonomous robots [1]. Lithium-ion batteries (LIB) have proved their reliability in many applications, such as uninterruptible power supply systems, photovoltaic power generation, energy recovery systems for industrial machinery, and transportation systems [1–3]. Nevertheless, huge research efforts are still concentrated on developing novel classes of electrode materials, mainly high voltage cathode ones. $LiFePO_4$ with olivine structure, which was first conveyed by Padhi et al. [4], has received excessive interest as LIB cathode material. It is one of the most promising materials amongst other olivines and is extensively studied due to low cost, high reversibility, thermal stability and safety [5]. However, $LiFePO_4$ has some deficiencies, such as low potential (3.4 V) and small packing density (owing to the inclusion of large-volume carbon), which lead to low specific energy density (580 W h·kg^{-1}).

To overcome these difficulties other transition metals were introduced in the olivine structure of $LiMPO_4$, M = Mn, Fe, Co, or Ni. Among them, $LiCoPO_4$ has a large theoretical capacity (167 mA h g^{-1}) and high specific energy density (800 W h·Kg^{-1}) [6]. This material has a high potential of 5.75 V as follows from theoretical GGA + U calculations [7] compared to 4.8 V vs. Li/Li$^+$ measured experimentally [8]. $LiCoPO_4$ was already applied in 18650 batteries, and Howard et al. appraised the $LiCoPO_4$ cost to be 142$ kW^{-1} h^{-1}, in comparison to 198 and 158$ k/Wh for $LiCoO_2$ and $LiFePO_4$ respectively [9,10]. Even though attractive for high energy and high power applications, large scale use of $LiCoPO_4$ as a cathode has been hindered by the unsatisfactory cycle stability and rate performance [10]. The latter fact was addressed theoretically and Osnis et al. showed that stability of $LiCoPO_4$ can be improved by Fe doping. In a mixed compound $LiFe_{1-y}Co_yPO_4$ the stability upon delithiation increases when Fe concentration increases [11].

The high cost of all Li-based batteries is related to the expensive sources of Li. Worldwide industrial applications of Li-based power sources lead to the shortage of Li raw materials and hence even higher production costs [12]. Higher abundance of Na in nature and its low cost

* Corresponding author. The Smart Materials Research Institute, Southern Federal University, Sladkova 178/24, 344090, Rostov-on-Don, Russia.
E-mail addresses: a.m.aboraia@gmail.com, mohamed@sfedu.ru (A.M. Aboraia).

https://doi.org/10.1016/j.jpcs.2019.109192
Received 26 April 2019; Received in revised form 23 August 2019; Accepted 8 September 2019
Available online 9 September 2019

lead to an advantage when a large amount of alkali is demanded for large-scale applications. Na-ion batteries can offer more energy density than Li-ion ones and can work at elevated temperatures [13]. For sodium-ion insertion, negative electrodes based on hard carbons have brilliant properties with up to 350 mA h g^{-1} capacity [14,15].

For the synthesis of $LiMPO_4$ materials (M = Fe, Co, Ni, Mn) many techniques were applied, such as sol-gel method [16,17], hydrothermal synthesis и [18], MW heating [19–21], and other [20,22–24]. For example, for $LiFePO_4$, one of common synthesis methods includes either solid-state approach and/or solution-based approach [23]. In the present work, we have used MW synthesis technique to reduce the time of heating and particle size. This strategy is robust not only for decreasing the time of reaction, but can also be adjusted in order to produce standardized nanoparticles on the industrial scale [25]. In conventional synthesis 3d metal phosphates with Na form an electrochemically inactive matricite structure which has no cationic sodium diffusion. In a solid state or mechanochemical reaction three phases – α, β and γ-NaCoPO4 can be obtained [26]. Recently Gutierrez et al. [27]synthesized electrochemically active Red-phase of $NaCoPO_4$ by microwave-assisted method. The material showed stable capacity in the range 35–40 mA h/g for the 40 cycles with a voltage range 4–4.5 V vs. Na/Na^+. The Red-phase categorizes as one of the very few high voltage cathodes presently available for sodium-ion batteries. Following the success of $LiMPO_4$ materials the similar Na-based compound with olivine structure, $NaMPO_4$ is a potential better candidate for sodium ion batteries.

In present work we have synthesized $NaCoPO_4$ both in β- and Pnma phases using protocol from $LiCoPO_4$ synthesis. From the theoretical point of view, we introduce a routine for practical construction of novel mixed $Li_xNa_{1-x}CoPO_4$ material by sequential substitution of Li to Na. We discuss its electrochemical properties and formation energies. GGA + U simulations for a large supercell of the $Li_{1-x}Na_xCoPO_4$ structure allowed accurate estimations of the volume changes and working potentials of the material. We show that introducing sodium in the structure of the material increases the operational voltage from vs. Na/Na^+. For the first time we calculated accurate Bader charges on all atoms in the unit cell and show their variation across the insertion and extraction cycles of lithium and sodium. We report the inherent relative stabilities of $Li_{1-x}Na_xCoPO_4$ and Li_xCoPO_4 (x = 0, 0.25,0.5,0.75, 1) and Na_xCoPO_4 (x = 0.25, 0.5, 0.75, 1) and show that sodium might play a significant role in the electrochemical performance of the cathode material.

2. Methods

Spin-polarized density functional calculations were performed with the VASP 5.2 program package via projector augmented wave (PAW) method. For every composition x,y in $Li_xNa_yCoPO_4$ cell volume and atomic positions were optimized in a two-step procedure. $2 \times 2 \times 1$ supercell with 112 atoms, constructed from the orthorhombic structure for $LiCoPO_4$ with Pnma space group [28] was used as an initial approximation. Then at a first step, lattice parameters were relaxed while unit cell angle and atomic positions were constrained to their initial values. In a second step, atomic positions were relaxed for fixed, optimized lattice parameters. A kinetic energy cutoff 520 eV was used for the plane-wave basis set. $3 \times 3 \times 3$ K-point meshes were automatically generated according to the Monokhorts-Pack scheme. The PBEsol functional [29] was used to treat exchange-correlation effects while on-site Coulomb interactions were corrected by the GGA + U approach via Dudarev scheme [30]. We used U = 5.05 eV for Co [7]. For optimized structures, we calculated atomic charges using Bader method. The Bader charge is calculated for the all-electron density recovered from the POTCAR file using the LAECHG = .TRUE [31]. keyword to obtain core electron densities from the calculation [32].

For synthesis the following starting materials were purchased from Alfa Aesar and used without purification: lithium phosphate monobasic LiH_2PO_4, sodium phosphate monobasic dihydrate $NaH_2PO_4{\cdot}2H_2O$, lithium acetate monohydrate $LiC_2H_3O_2{\cdot}H_2O$ (LiAc), sodium acetate monohydrate $NaC_2H_3O_2$ (NaAc), cobalt(II) oxalate dihydrate $CoC_2O_4{\cdot}2H_2O$ (CoOx), glucose $C_6H_{12}O_6$, ethylene glycol (EG). Ultrapure water (18 MΩ cm) was produced by SimplicityUV (Millipore) from distilled water. In a typical synthesis Li(Na)H2PO4, Li(Na)Ac, CoOx and glucose were dissolved in water. Then EG was added, and the reaction mixture was placed into Teflon vessel, closed hermetically and heated in MW oven CEM Mars 6 at 220 °C for 3 h with magnetic stirring. Molar ratio of mixture components was Li(Na)H_2PO_4:Li(Na)Ac:CoOx:glucose:water:EG = 1.17:1.83:1:0.57:240.8:119.4. After cooling down precipitate was separated by centrifugation at 20000 rpm, washed with water three times and dried at 60 °C overnight. The as-synthesized powders were annealed in air at 700 °C for 8 h.

Powder XRD patterns were collected with a laboratory Bruker D2 Phaser diffractometer using Cu $K\alpha_1$ radiation in the 5°–89° 2θ range. The XRD patterns were analyzed by means of Rietveld refinement in FullProf software [33]. Co K-edge X-ray absorption near edge spectra (XANES) of $LiCoPO_4$ and $NaCoPO_4$ samples were measured with Rigaku R-XAS Looper laboratory spectrometer. All measurements were performed in transmission geometry with Ge (311) crystal as a monochromator, providing energy resolution ΔE = 1.9 eV. The incident beam intensity was measured by Ar-filled (300 mbar) ionization chamber, transmitted intensity – by scintillation counter with a photomultiplier tube. The samples for measurements were diluted with 50 mg of dry cellulose powder and pressed into pellets. The amount of sample for a pellet was calculated using XAFSmass software [34]. Spectra for reference compounds (CoO, Co_3O_4) were measured the same way to determine the charge state of Co using the chemical shift rule.

3. Results and discussion

Fig. 1 shows the XRD patterns of the synthesized materials. After reactions we obtained Pnma phase for $LiCoPO_4$ with lattice parameters 10.22, 5.93 and 4.71 Å which are consistent with previously reported results [35]. $NaCoPO_4$ has two phases as shown in Fig. 1b. The first phase has Pnma symmetry and the second has $P6_5$ symmetry and different lattice parameters.

Experimental lattice parameters for the as synthesized sample were further confirmed by means of theoretical DFT calculations. Table 1 shows a comparison between the calculated lattice parameters and experimental ones. The difference between experimental and theoretical lattice parameters for $LiCoPO_4$ is about 0.2% which is in the order of magnitude of the accuracy of DFT GGA-PBE approximation. For $NaCoPO_4$ we observe larger differences between experimental data and calculations due to different stoichiometry observed in the synthesized samples – i.e. real composition of synthesized material was Na_xCoPO_4 with x < 1. We further confirm this fact by using Co K-edge XANES spectroscopy.

Due to higher ionic radius insertion of Na in the cathode material increases the cell parameters of the system. The cell volume per formula unit for $NaCoPO_4$ reaches 303.396 $Å^3$ and is larger than one of $LiCoPO_4$ by 6.2%. These results agree with the difference between ionic radii of Li and Na which is 74.5%. Unit cell volumes for the $LiNaCoPO_4$ system with different concentrations of alkali metals are shown in Fig. 2. The calculation reproduces the experimental structural parameters of pure $LiCoPO_4$ with the accuracy of 0.2%. As shown in Table 1, the volume of Li_xCoPO4 increases along with the ratio of Li by 0.37% between x = 0.25 and 0.5, and by 0.26% between x = 0.5 and 0.75, but for x from 0.75 to 1 the change is very insignificant. These results agree with in situ XRD measurements obtained by Ref. [35].

The chemical bond energies were calculated using Equation (1), where E(Li), E(Co), are the total energies calculated for a single atom in the supercell. For instance, the chemical bond energy for 2x2 $LiCoPO_4$ supercell can be calculated according to the following equation:

$$\Delta E = E(Li_xCoPO_4) - x{\cdot}E(Li) - 16{\cdot}E(Co) - 16{\cdot}E(P) - 64{\cdot}E(O) \quad (1)$$

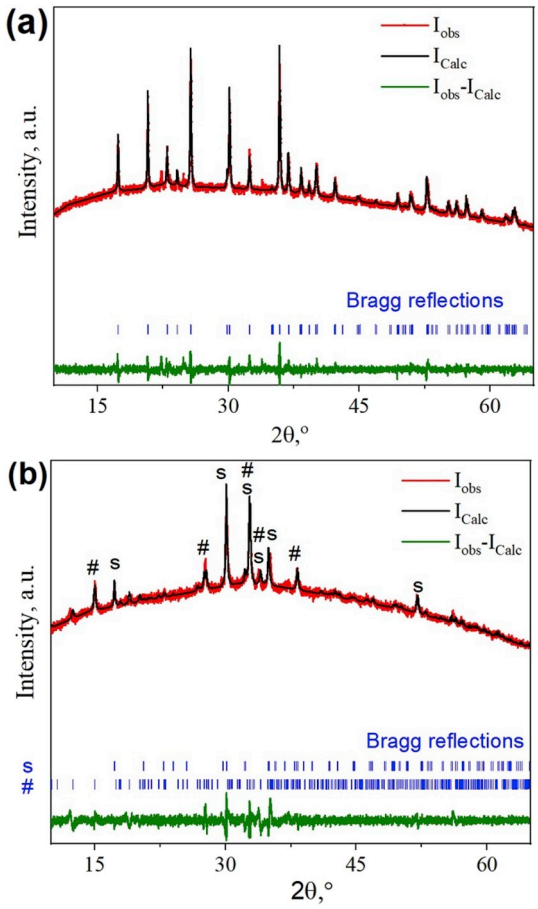

Fig. 1. Experimental powder XRD patterns for the synthesized $LiCoPO_4$ (a) and $NaCoPO_4$ (b) after annealing along with results of Rietveld refinement. Single orthorhombic phase was used for $LiCoPO_4$ and olivine structure of $NaCoPO_4$ was fitted with two phases (*s* and # stand for Pnma and β-$NaCoPO_4$) reported in Ref. [36].

Table 1
Comparison of the calculated unit cell parameters of Li_xCoPO_4, Na_xCoPO_4 and $Li_xNa_yCoPO_4$ for Pnma space group and refined experimental values.

Li_xNa_yCoPO4		a (Å)	b (Å)	c (Å)	V(Å^3)
x (Li)	y (Na)	Theory			
1.00	0.00	10.202	5.918	4.708	284.303
0.75	0.00	10.201	5.918	4.708	284.281
0.50	0.00	10.192	5.913	4.704	283.541
0.25	0.00	10.179	5.905	4.698	282.465
0.00	1.00	10.425	6.047	4.812	303.396
0.00	0.75	10.361	6.011	4.782	297.886
0.00	0.50	10.277	5.962	4.744	290.707
0.00	0.25	10.215	5.926	4.715	285.420
0.75	0.25	10.301	5.976	4.755	292.744
0.50	0.50	10.323	5.99	4.765	294.589
0.25	0.75	10.418	6.043	4.808	302.771
0.25	0.50	10.301	5.976	4.754	292.709
0.50	0.25	10.240	5.940	4.726	287.496
0.25	0.25	10.220	5.928	4.717	285.837
Experiment					
$LiCoPO_4$		10.22	5.93	4.71	285.44
$NaCoPO_4$		10.26	5.93	4.74	288. 39
		10.16	10.16	23.87	2463.99

where *x* is the number of Li atoms in the supercell. This value is further divided by 16 to obtain bond energy per formula unit. To obtain the intercalation energies for different stoichiometries and hence the

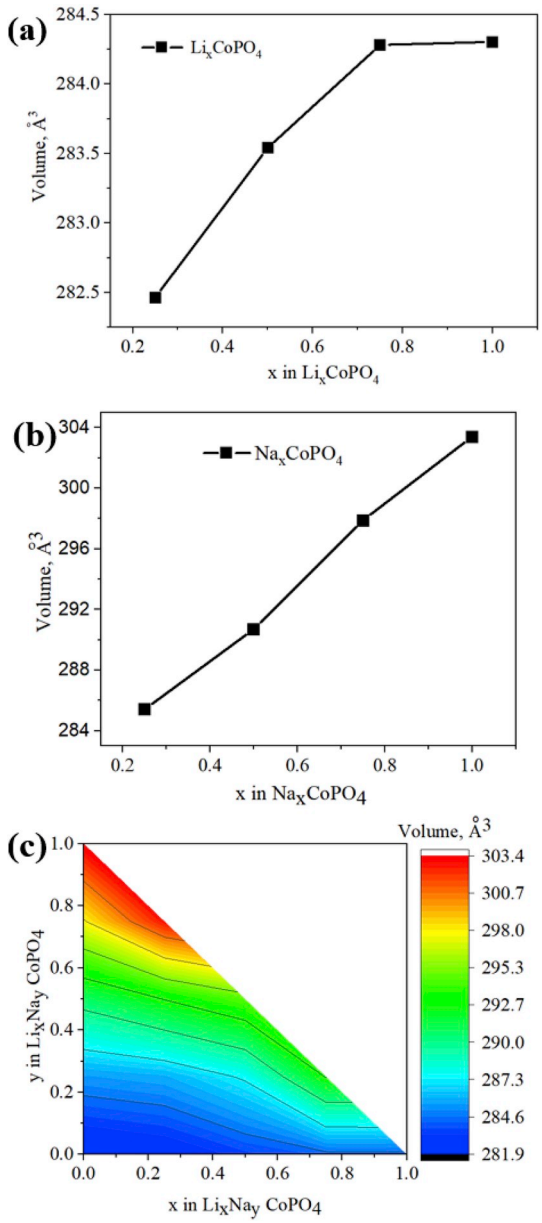

Fig. 2. Calculated volume of the unit cell as a function of alkali metal concentration x for (a) Li_xCoPO_4 (b) Na_xCoPO_4 and (c) $Li_xNa_yCoPO_4$.

working cell potential we utilized following reactions:

$$CoPO4 + xLi_{(s)} \rightarrow Li_xCoPO_4$$

$$CoPO4 + Na_{1-x} + xLi_{(s)} \rightarrow Li_xNa_{1-x}CoPO_4 \quad (2)$$

$$CoPO4 + xNa_{(s)} \rightarrow Na_xCoPO_4$$

Where energies for Na and Li were calculated for metallic species. From Fig. 3a the chemical bond energy per formula unit for Li_xCoPO_4 equals −35.31 eV when x = 1. When 25% of lithium has been removed the value increased by 1.56 eV per formula unit indicating decreasing of the stability. Similarly, when 25% of Na were removed from $NaCoPO_4$ the resulting value of chemical bond energy increased by 1.53 eV per formula unit. That means the $LiCoPO_4$ and $NaCoPO_4$ show similar behavior.

During charge lithium ions are extracted from the $LiCoPO_4$ cathode material and deposited on the metallic Li anode. During the discharge, Li-ions are removed from the anode to cathode. Aydinol et al. [37] presented a theoretical method for calculation of the average voltage of

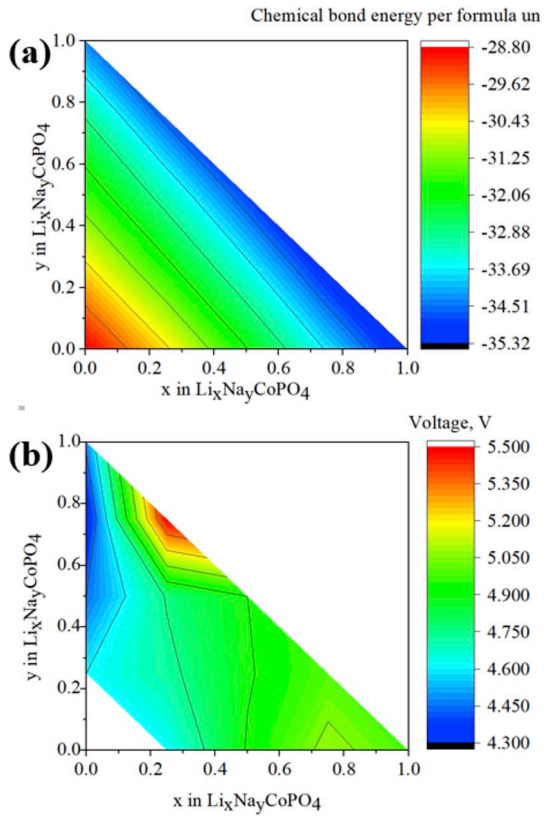

Fig. 3. Energetics of the delithiation process of $Li_xNa_yCoPO_4$. (a) The chemical bond energy calculated according to equation (2) per formula unit for Li_xNa_y-$CoPO_4$, where (x = 0, 0.25, 0.5, 0.75 and 1), (y = 0, 0.25, 0.5, 0.75 and 1). (b) Corresponding voltage profile during delithiation process in $Li_xNa_yCoPO_4$ calculated according to equation (3).

delithiation for the Li-ion cell. We applied this technique for $LiCoPO_4$, Na_xCoPO4 and $Li_xNa_{1-x}CoPO_4$. The average lithiation/delithiation voltage (vs Li/Li+) can be calculated using the Gibbs energy per Li added/removed during the reaction, as shown in Equation (3) [38].

$$V = \frac{-\Delta G}{F \cdot \Delta N_{Li}} \tag{3}$$

where F is the Faraday constant, ΔN_{Li} is the amount of Li added/removed, and ΔG_f is the change in the Gibbs free energy due to intercalation which can be approximated by the intercalation energy from equation (2) [38]:

$$\Delta G \approx E_{int} = \frac{E(LiCoPO_4) - E(CoPO_4) - n \cdot E(Li)}{N_{Li}} \tag{4}$$

As follows from Fig. 3b the average voltage before delithiation for $LiCoPO_4$ equals 4.99 V vs. Li/Li^+ but after delithiation decreases to 4.61 V vs. Li/Li^+ close to experimental value 4.8 V vs Li/Li+ [39]. On the other hand, the calculated voltage of $NaCoPO_4$ reaches 4.48 V Na/Na^+ as shown in Fig. 3b in agreement with the voltage value obtained by Gutierrez et al. [27]. However, upon a decrease in the amount of sodium down to 0.75 the voltage decreases to 4.30 V vs. Na metal, and increases to 4.45 V when y = 0.5 as shown in Fig. 3b. When we exchange 50% of Na by 50% of Li the calculated intercalation voltage of $Li_{0.5}Na_{0.5}CoPO_4$ equals to 4.9 V vs. Li/Li^+.

To analyze changes in atomic charges we have performed the Bader charge analysis for all atoms in the supercell upon discharge process. The analysis proves that the cobalt formal charge state can be assigned to Co^{2+} for all atoms when x = 1 in Li_xCoPO_4 as shown in Fig. 4a. Upon Li removal, the corresponding number of Co atoms change their oxidation state to +3. This fact is indicated by a vertical error bar in

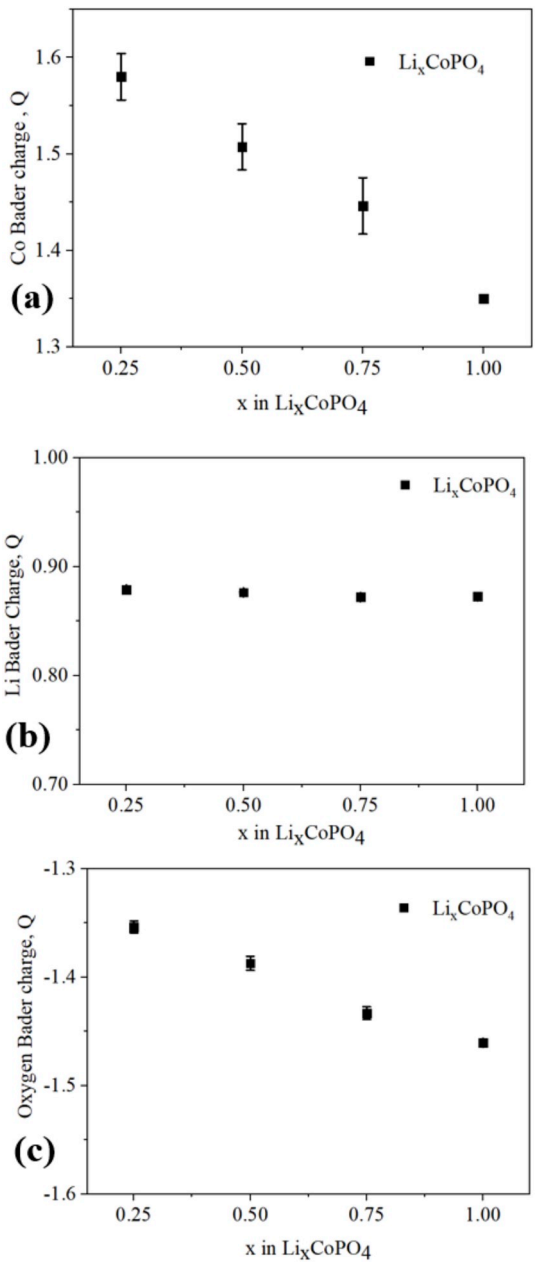

Fig. 4. (a) Calculated average Bader charge on Co atoms with respect to different ratio of Li in $LiCoPO_4$ supercell. Panels (b) and (c) show calculated average Bader charges on Li and oxygen atoms in the same cell. The error bars indicate variations of atomic charges within the supercell and they are largest for Co due to coexistence of Co^{2+}/Co^{3+} ions.

Fig. 4a after averaging the Co Bader charge for all atoms in the supercell. The oxidation state of Co in Li_xCoPO_4 and Na_xCoPO_4 has the same behavior as shown in Figs. 4a and 5a. Particular emphasis should be focused on the fact that we observed variations also in oxygen Bader charge upon variation of Li and Na content in the unit cell. This effect is related to the redistribution of the electron density in the first coordination shell of Co upon transition from +2 to +3 charge state as shown in Fig. 6.

As shown in Fig. 7a experimental Co K-edge XANES spectrum for $LiCoPO_4$ matches the energy position of CoO therefore oxidation state of Co can be estimated as Co^{2+}. Fig. 7b compares experimental Co K-XANES spectra for $LiCoPO_4$ and $NaCoPO_4$. The overall similarity of these spectra suggests similar olivine structure for both phases. However, there are also important differences. $NaCoPO_4$ demonstrates the lower

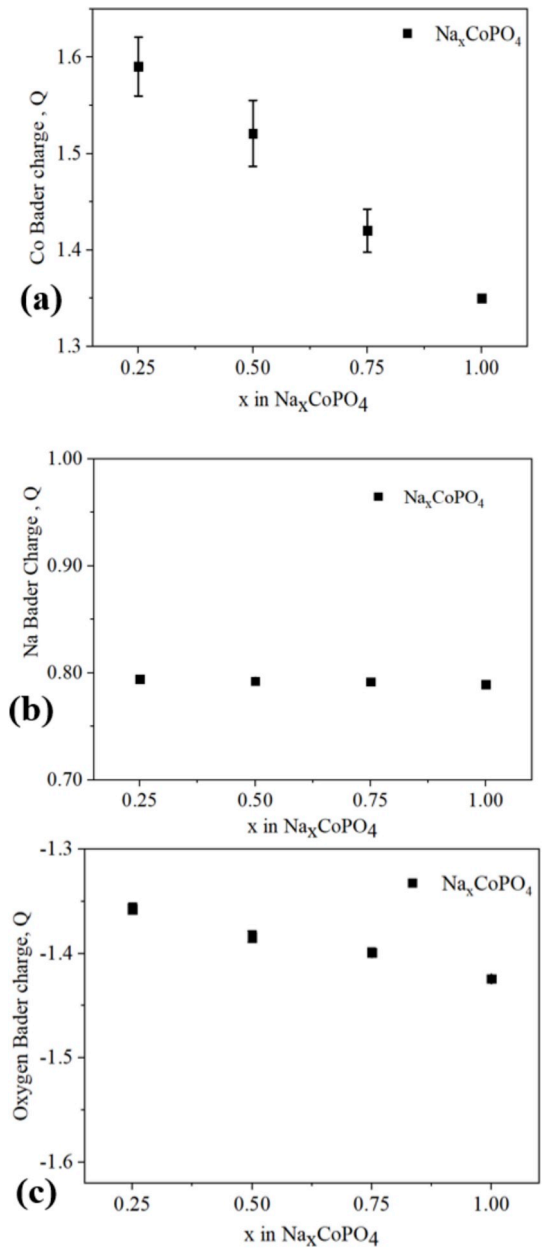

Fig. 5. The same as Fig. 4 but for $NaCoPO_4$. (a) Calculated average Bader charge on Co atoms with respect to different ratio of Li in $LiCoPO_4$ supercell. Panels (b) and (c) show calculated average Bader charges on Li and oxygen atoms in the same cell. The error bars indicate variations of atomic charges within the supercell and they are largest for Co due to coexistence of Co^{2+}/ Co^{3+} ions.

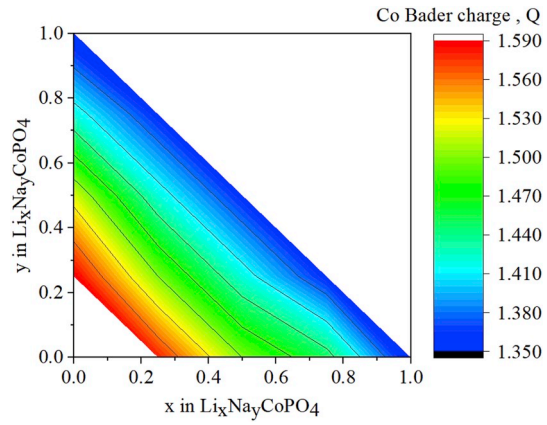

Fig. 6. Variation of the average cobalt charge with respect to different ratio of Li and Na in $Li_xNa_yCoPO_4$ supercell.

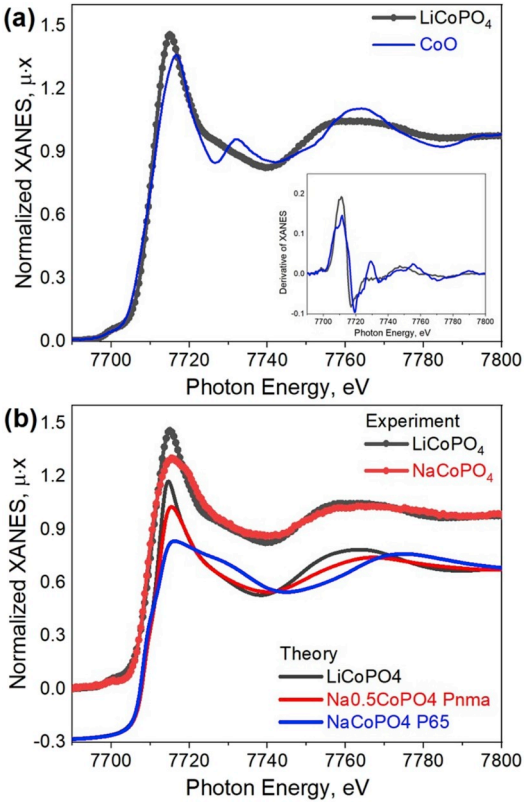

Fig. 7. Co K-edge XANES spectra. (a) The experimental Co K-edge XANES spectra for $LiCoPO_4$ and CoO (b) comparison between experimental spectra for $LiCoPO_4$ and $NaCoPO_4$ with theoretical simulations for $LiCoPO_4$ Pnma phase (black), optimized 2x2 $Na_{0.5}CoPO_4$ supercell with Pnma phase (red) and $NaCoPO_4$ with $P6_5$ phase (blue).

intensity and broader main peak located at 7720 eV, which is indicative for the mixture of phases and distortions in the first coordination sphere of Co and for possible presence of two phases in agreement with XRD analysis (refined Pnma and $P6_5$ space groups). Fig. 7b contains theoretical simulations for pure $LiCoPO_4$ and two phases of $NaCoPO_4$: $Na_{0.5}CoPO_4$ in Pnma space group and $NaCoPO_4$ with $P6_5$ space group. Sharp features of $LiCoPO_4$ XANES show good agreement with theoretical simulation thus suggest that it contains only one phase in accordance to XRD data analysis. Simulations for $Na_{0.5}CoPO_4$ indicate that lower intensity of the main edge at 7715 eV and broad feature at 7760 eV arise from multiple superposition of spectra for Co^{2+} and Co^{3+} positions in the supercell (see Fig. S1 for spectra of inequivalent Co positions in the supercell). Tetrahedral coordination of Co in $P6_5$ phase (bottom blue curve) can be also responsible for the observed differences between $NaCoPO_4$ and $LiCoPO_4$.

Experimental spectra for $LiCoPO_4$ and $NaCoPO_4$ show similar positions of the absorption edge. Our model for $NaCoPO_4$ includes phase with reduced stoichiometry of Na – i.e. $Na_{0.5}CoPO_4$. Higher average Co oxidation state in this phase should result in absorption edge shift which is not observed experimentally. We attribute this fact to the two effects which affect absorption edge position. First is the Co charge state. Second is the Co–O interatomic distances in the first coordination sphere. The latter decrease upon Co^{2+} - Co^{3+} transition. This effect can partially compensate the expected absorption edge shift. Experimental studies of

$NaCoPO_4$ upon cycling also indicate small edge shift between fully charged and fully discharges samples [27].

From the above we confirmed that parameters of the synthesis used for $LiCoPO_4$ can be applied to obtain olivine phase of $NaCoPO_4$. Therefore electrochemical performance of $NaCoPO_4$ can be expected to be similar to the one obtained for LiCoPO4 and can be further improved via the same routes used for $LiCoPO_4$ such as: coating the $NaCoPO_4$ by homogeneous layer of carbon or doping the active material by transition metal [40]. Carbon could act as a reductant to avoid the formation of undesirable impurities, and on the other hand, carbon could act as a nucleating agent to decrease the particle size of the final material (shorter diffusion lengths and a larger electrolyte/electrode contact area) [41].

4. Conclusion

We have synthesized both $LiCoPO_4$ and $NaCoPO_4$ via rapid low-temperature MW-assisted solvothermal approach. Optimal synthesis parameters provided $LiCoPO_4$ with orthorhombic phase and Pnma space group, while $NaCoPO_4$ has two phases with different space groups (Pnma and P65) which are both expected to be electrochemically active. By means of X-ray diffraction and DFT calculations, we have analyzed the crystal structure for both materials and revealed that stoichiometry of Na in $NaCoPO_4$ is reduced due to the presence of Na vacancies in the material. The presence of Na vacancies is further supported by Co K-edge XANES which revealed the distortions in the local coordination of Co due to coexistence of Co^{2+} and Co^{3+} sites. DFT simulations for the supercell during the delithiation process predict a decrease of the cell volume of Li_xCoPO_4 and Na_xCoPO_4 along with the Li or Na content. The $LiCoPO_4$ and $NaCoPO_4$ show similar behaviuor for chemical bond energy: upon removing 25% of Li the bond energy increases by1.56 eV per formula unit. Therefore, $NaCoPO_4$ or mixed $Li_xNa_yCoPO_4$ can be electrochemically prepared starting from the $LiCoPO_4$ by substituting alkali metals. The calculated voltage for $LiCoPO_4$ is 4.6 V and does not vary much across the Li concentration in the cell, which is close to the experimental value of 4.8 V. The theoretical voltage for $NaCoPO_4$ is 4.48 V comparable with the experimental one, theoretical voltage for $Li_{0.5}Na_{0.5}CoPO_4$ is 4.9V.

Acknowledgements

The authors acknowledge the Deanship of Scientific Research at King Khalid University for funding this work through research groups program under grant number R.G.P.1/12/39. A.V.S. acknowledges a support from grant of the RFBR for X-ray absorption measurements and analysis according to the research project No 17-02-01350\17.

Appendix A. Supplementary data

Supplementary data to this article can be found online at https://doi.org/10.1016/j.jpcs.2019.109192.

References

[1] M.S. Whittingham, Lithium batteries and cathode materials, Chem. Rev. 104 (10) (2004) 4271–4301.
[2] J.W. Fergus, Recent developments in cathode materials for lithium ion batteries, J. Power Sources 48 (4) (2010) 939.
[3] M.R. Palacin, ChemInform abstract: recent advances in rechargeable battery materials: a Chemist's perspective, ChemInform 40 (47) (2009) 2565–2575.
[4] A.K. Padhi, K.S. Nanjundaswamy, J.B. Goodenough, Phospho-olivines as positive-electrode materials for rechargeable lithium batteries, J. Electrochem. Soc. 144 (4) (1997) 1188–1194.
[5] S.K. Martha, et al., LiMn0.8Fe0.2PO4: an advanced cathode material for rechargeable lithium batteries, Angew. Chem. Int. Ed. 48 (45) (2009) 8559–8563.
[6] D. Liu, et al., High-energy lithium-ion battery using substituted LiCoPO4: from coin type to 1 Ah cell, J. Power Sources 388 (2018) 52–56. February.
[7] X.H. Zhu, N. Chen, F. Lian, Y.P. Song, Y. Li, First principle calculation of lithiation/delithiation voltage in Li-ion battery materials, Chin. Sci. Bull. 56 (30) (2011) 3229–3232.
[8] S. Brutti, et al., Controlled synthesis of LiCoPO4 by a solvo-thermal method at 220 °c, Mater. Lett. 145 (2015) 324–327.
[9] W.F. Howard, R.M. Spotnitz, Theoretical evaluation of high-energy lithium metal phosphate cathode materials in Li-ion batteries, J. Power Sources 165 (2) (2007) 887–891.
[10] M. Zhang, N. Garcia-Araez, A.L. Hector, Understanding and development of olivine LiCoPO4 cathode materials for lithium-ion batteries, J. Mater. Chem. A 6 (30) (2018) 14483–14517.
[11] A. Osnis, M. Kosa, D. Aurbach, D.T. Major, Systematic first-principles investigation of mixed transition metal olivine phosphates LiM 1, J. Phys. Chem. C 117 (2013) 17919–17926.
[12] M. Ramzan, R. Ahuja, Ferromagnetism in the potential cathode material LiNaFePO4F, Epl 87 (1) (2009).
[13] P.K. Nayak, L. Yang, W. Brehm, P. Adelhelm, From lithium-ion to sodium-ion batteries: advantages, challenges, and surprises, Angew. Chem. Int. Ed. 57 (1) (2018) 102–120.
[14] D.A. Stevens, J.R. Dahn, The mechanisms of lithium and sodium insertion in carbon materials, J. Electrochem. Soc. 148 (8) (2001) 803–811.
[15] D.A. S, J.R. Dahn, High capacity anode materials for rechargeable sodium-ion batteries, J. Electrochem. Soc. 147 (4) (2000) 1271–1273.
[16] Y. Wang, Y. Wang, E. Hosono, K. Wang, H. Zhou, The design of a LiFePO4/carbon nanocomposite with a core–shell structure and its synthesis by an in situ polymerization restriction method, Angew. Chem. Int. Ed. 47 (39) (2008) 7461–7465.
[17] S. Jiang, Y. Wang, Synthesis and characterization of vanadium-doped LiFePO 4 @C electrode with excellent rate capability for lithium-ion batteries, Solid State Ion. 335 (January) (2019) 97–102.
[18] J. Chen, M.J. Vacchio, S. Wang, N. Chernova, P.Y. Zavalij, M.S. Whittingham, The hydrothermal synthesis and characterization of olivines and related compounds for electrochemical applications, Solid State Ion. 178 (31–32) (2008) 1676–1693.
[19] A.V. Murugan, T. Muraliganth, A. Manthiram, Comparison of microwave assisted solvothermal and hydrothermal syntheses of LiFePO4/C nanocomposite cathodes for lithium ion batteries, J. Phys. Chem. C 112 (37) (2008) 14665–14671.
[20] Z.H.S.M. Masoudpanah, CTAB-assisted solution combustion synthesis of LiFePO 4 powders, J. Sol. Gel Sci. Technol. (2019) 335–341.
[21] A. Örnek, Positive effects of a particular type of microwave-assisted methodology on the electrochemical properties of olivine LiMPO4 (M = Fe, Co and Ni) cathode materials, Chem. Eng. J. 331 (2018) 501–509.
[22] K.S. Park, J.T. Son, H.T. Chung, S.J. Kim, C.H. Lee, H.G. Kim, Synthesis of LiFePO 4 by co-precipitation and microwave heating, Electrochem. Commun. 5 (10) (2003) 839–842.
[23] E.J. Shin, et al., A green recycling process designed for LiFePO4 cathode materials for Li-ion batteries, J. Mater. Chem. A 3 (21) (2015) 11493–11502.
[24] Y. Li, I. Taniguchi, Facile synthesis of spherical nanostructured LiCoPO4 particles and its electrochemical characterization for lithium batteries, Adv. Powder Technol. 30 (8) (2019) 1434–1441.
[25] J.-J. Choi, et al., Synthesis of nanostructured Li 2 MnSiO 4/C using a microwave assisted sol–gel process with water as a base solvent, J. Electroceram. 31 (1–2) (2013) 176–180.
[26] S.-N. Le, H.W. Eng, A. Navrotsky, Energetics of cobalt phosphate frameworks: **a, b**, and red NaCoPO4, YJSSC J. Solid State Chem. 179 (12) (2006) 3731–3738.
[27] A. Gutierrez, S. Kim, F. TT, J. C.S, Microwave-assisted synthesis of NaCoPO4 red-phase and initial characterization as high voltage cathode for sodium-ion batteries, ACS Appl. Mater. Interfaces 9 (5) (2017) 4391–4396.
[28] Y.M. Kang, et al., Structurally stabilized olivine lithium phosphate cathodes with enhanced electrochemical properties through Fe doping, Energy Environ. Sci. 4 (12) (2011) 4978–4983.
[29] S.L. Shang, Y. Wang, Z.G. Mei, X.D. Hui, Z.K. Liu, Lattice dynamics, thermodynamics, and bonding strength of lithium-ion battery materials LiMPO 4 (M = Mn, Fe, Co, and Ni): a comparative first-principles study, J. Mater. Chem. 22 (3) (2012) 1142–1149.
[30] T. Kimura, C. Chang, F. Kimura, M. Maeyama, The pseudo-single-crystal method: a third approach to crystal structure determination, J. Appl. Crystallogr. 42 (3) (2009) 535–537.
[31] M. Kosa, D.T. Major, Structural trends in hybrid perovskites [Me 2 NH 2] M [HCOO] 3 (M= Mn, Fe, Co, Ni, Zn): computational assessment based on Bader charge analysis, CrystEngComm 17 (2) (2015) 295–298.
[32] S. Sun, et al., Monodisperse MFe2O4 (M = Fe, Co, Mn) nanoparticles, J. Am. Chem. Soc. 126 (1) (2004) 273–279.
[33] V. V Butova, et al., Zn/Co ZIF family: MW synthesis, characterization and stability upon halogen sorption, Polyhedron 154 (2018) 457–464.
[34] K. Klementiev, R. Chernikov, XAFSmass: A program for calculating the optimal mass of XAFS samples, J. Phys. Conf. Ser. 712 (1) (2016) 1–5.
[35] K.J. Kreder, G. Assat, A. Manthiram, Microwave-assisted solvothermal synthesis of three polymorphs of $LiCoPO_4$ and their electrochemical properties, Chem. Mater. 27 (16) (2015) 5543–5549.
[36] R. Hammond, J. Barbier, Structural chemistry of NaCoPO4, Acta Crystallogr. Sect. B Struct. Sci. 52 (3) (1996) 440–449.
[37] M.K. Aydinol, A.F. Kohan, G. Ceder, Ab initio calculation of the intercalation voltage of lithium-transition-metal oxide electrodes for rechargeable batteries, J. Power Sources 68 (2) (1997) 664–668.

[38] G. Ramos-Sanchez, A. Callejas-Tovar, L.G. Scanlon, P.B. Balbuena, DFT analysis of Li intercalation mechanisms in the Fe-phthalocyanine cathode of Li-ion batteries, Phys. Chem. Chem. Phys. 16 (2) (2014) 743–752.
[39] H.H. Li, J. Jin, J.P. Wei, Z. Zhou, J. Yan, Fast synthesis of core-shell LiCoPO4/C nanocomposite via microwave heating and its electrochemical Li intercalation performances, Electrochem. Commun. 11 (1) (2009) 95–98.
[40] H.H. Li, J. Jin, J.P. Wei, Z. Zhou, J. Yan, Fast synthesis of core-shell LiCoPO4/C nanocomposite via microwave heating and its electrochemical Li intercalation performances, Electrochem. Commun. 11 (1) (2009) 95–98.
[41] L.X. Yuan, et al., Development and challenges of LiFePO4 cathode material for lithium-ion batteries, Energy Environ. Sci. 4 (2) (2011) 269–284.